



Prospects for improved seasonal Arctic sea ice predictions from multivariate data assimilation



François Massonnet*, Thierry Fichefet, Hugues Goosse

Georges Lemaître Centre for Earth and Climate Research, Earth and Life Institute, Université catholique de Louvain, Louvain-la-Neuve, Belgium

ARTICLE INFO

Article history:

Received 28 May 2014

Received in revised form 16 December 2014

Accepted 21 December 2014

Available online 18 February 2015

Keywords:

Sea ice

Seasonal prediction

Data assimilation

Ensemble Kalman filter

Ocean–sea ice modeling

Initialization

ABSTRACT

Predicting the summer Arctic sea ice conditions a few months in advance has become a challenging priority. Seasonal prediction is partly an initial condition problem; therefore, a good knowledge of the initial sea ice state is necessary to hopefully produce reliable forecasts. Most of the intrinsic memory of sea ice lies in its thickness, but consistent and homogeneous observational networks of sea ice thickness are still limited in space and time. To overcome this problem, we constrain the ocean–sea ice model NEMO-LIM3 with gridded sea ice concentration retrievals from satellite observations using the ensemble Kalman filter. No sea ice thickness products are assimilated. However, thanks to the multivariate formalism of the data assimilation method used, sea ice thickness is globally updated in a consistent way whenever observations of concentration are available. We compare in this paper the skill of 27 pairs of initialized and uninitialized seasonal Arctic sea ice hindcasts spanning 1983–2009, driven by the same atmospheric forcing as to isolate the pure role of initial conditions on the prediction skill. The results exhibit the interest of multivariate sea ice initialization for the seasonal predictions of the September ice concentration and are particularly encouraging for hindcasts in the 2000s. In line with previous studies showing the interest of data assimilation for sea ice thickness reconstruction, our results thus show that sea ice data assimilation is also a promising tool for short-term prediction, and that current seasonal sea ice forecast systems could gain predictive skill from a more realistic sea ice initialization.

© 2015 Elsevier Ltd. All rights reserved.

1. Introduction

Seasonal predictions of the summer Arctic sea ice cover are regarded by many as a valuable source of information for economic, strategic or societal reasons (AMAP, 2011). There exists several approaches to make such predictions, including heuristic statements, public surveys, statistical inference from empirical relationships and dynamical forecasting. The Sea Ice Outlook initiative (<http://www.arcus.org/search/seaiceoutlook>) provides a good overview of the status of current efforts. However, as outlined by Stroeve et al. (2014), the skill of the predictions is generally low when the observed sea ice cover departs significantly from the trend line, meaning that more research is needed before reliable forecasts can be issued on an operational basis. Predictions obtained from ocean–sea ice models (Zhang et al., 2008; Lindsay et al., 2012), or from fully-coupled general circulation models (GCMs) (Wang et al., 2012; Chevallier et al., 2013; Sigmond et al., 2013), deserve particular interest. Indeed, in the rapidly changing

Arctic environment, past statistical relationships may not hold (Holland and Stroeve, 2011) so that empirically-based predictions may be of limited use for the coming years or decades.

Because of the time scales involved, seasonal Arctic sea ice prediction with climate models requires a good knowledge of both initial and boundary conditions. As an example, Kauker et al. (2009) estimated that the September 2007 sea ice area anomaly was in part (66%) determined by past ocean and sea ice conditions in June, the rest of the anomaly being attributed to the integrated effects of atmospheric conditions between June and September. Consequently, a dynamical forecast system that seeks to predict summer Arctic sea ice conditions should, at least, rely on realistic initial conditions. Specifically, a significant part of the predictability of summer Arctic sea ice is associated to its initial thickness (Holland and Stroeve, 2011; Chevallier and Salas Méria, 2012; Wang et al., 2012). The probability that a parcel of ice melts at the end of summer is indeed closely related to its thickness in winter (Maslanik et al., 2007; Goosse et al., 2009).

Several studies have made use of sea ice thickness products to directly constrain sea ice models (Mathiot et al., 2012; Lindsay et al., 2012; Lisæter et al., 2007). Most of the products (see for example the compilation listed by Lindsay, 2013) suffer from

* Corresponding author. Tel.: +32 10 47 30 67.

E-mail address: francois.massonnet@uclouvain.be (F. Massonnet).

URL: <http://www.climate.be/ufmasson> (F. Massonnet).

undersampling in space and/or time, allowing only for corrections of sea ice thickness in the vicinity of the measurements, and only when these measurements are conducted. Because of their wide coverage, satellite-based retrievals of sea ice thickness bear probably the greatest promise for initializing the sea ice cover in large-scale models. However, satellites monitor sea ice freeboard or draft, rather than thickness directly. To retrieve sea ice thickness, the thickness of snow on sea ice and values for snow and ice densities must be known; they are often taken climatological or constant (Kwok et al., 2008; Laxon et al., 2013). Although very valuable, satellite products for ice thickness are therefore still subject to substantial uncertainties and biases (Zygmuntowska et al., 2014; Schweiger et al., 2011).

Alternatively, sea ice concentration products can also be used to constrain sea ice models. Passive microwave measurements of sea ice concentration made by satellites are not free of errors (Eastwood et al., 2011), but benefit from a much better spatial and temporal coverage than observations of sea ice thickness. In this work, we propose to indirectly initialize sea ice thickness by the assimilation of sea ice concentration, using the ensemble Kalman filter (EnKF) in the global ocean–sea ice model NEMO-LIM3. Contrary to simple nudging, this filter updates all ocean and sea ice variables as long as they are related to the assimilated variable – here, sea ice concentration. Thus, following this so-called “multivariate” scheme, sea ice thickness can be updated continuously all over the Arctic basin, an achievement that would not have been possible based on thickness data only given the substantial inhomogeneities. The interest of such a multivariate approach for sea ice thickness has already been demonstrated for both Arctic and Antarctic sea ice (Lisæter et al., 2003; Mathiot et al., 2012; Massonnet et al., 2013). Continuing the work initiated by these studies, the present paper provides further perspectives for this data assimilation method in the particular case of seasonal prediction.

The ocean–sea ice model and the data assimilation method are presented in Section 2. We explain why the EnKF is an appropriate methodology when one or several variables are difficult to observe directly, or suffer from undersampling. We extract, from the data assimilation run, a set of 27 March initial states between 1983 and 2009, that are used as initial conditions for 27 seasonal Arctic sea ice prediction experiments, or simply “hindcasts”. It is worth noting that we run these hindcasts with assimilation turned off, but under prescribed atmosphere, as we wish to test the pure sensitivity of sea ice to its initial conditions. We assess the skill of these initialized seasonal hindcasts against the skill of uninitialized seasonal hindcasts in Section 3. The initialized simulations are found to be more skillful than uninitialized ones for the months of August and September, with clearer improvements over 2000–2009 than 1983–1999. We discuss these results in light of differences in the sea ice and ocean initial states in Section 4, with a focus on the year 2007 – the minimum sea ice extent of the time series. We close with a conclusion in Section 5.

2. Data and methods

2.1. General model configuration

NEMO-LIM3 is a global ocean–sea ice model, consisting of the ocean model OPA9 (Madec, 2008) coupled to the Louvain-la-Neuve sea ice model, version 3 (LIM3, Vancoppenolle et al., 2009). OPA9 is a finite difference, hydrostatic, primitive equation oceanic GCM designed for climate studies. OPA9 runs on the ORCA2 grid ($\sim 2^\circ$ resolution), with mesh refinement around the equator and at the poles. The sea ice model LIM3 explicitly resolves the sub-grid scale sea ice thickness distribution using five ice

categories with lower bounds equal to 0, 0.63, 1.33, 2.25 and 3.84 m, respectively. The interested reader is redirected to Madec (2008) and Vancoppenolle et al. (2009) for a detailed description of the ocean and sea ice models.

The ocean–sea ice model is driven by atmospheric reanalyses and climatologies. The 2-m surface air temperatures and 10-m winds from the NCEP/NCAR reanalysis project (Kalnay et al., 1996) force the model on a daily basis and vary from year to year. Monthly climatologies of relative humidity (Trenberth et al., 1989), total cloudiness (Berliand and Strokina, 1980) and precipitation (Large and Yeager, 2004) complete the forcing. We follow the formulation described in Goosse, 1997 to compute the atmosphere–sea ice and atmosphere–ocean turbulent and radiative fluxes. River runoff rates are taken from the climatological dataset of Baumgartner and Reichel, 1976 combined with a mean seasonal cycle derived from the Global Runoff Data Centre data (GRDC, 2000).

2.2. Sea ice data assimilation

The ensemble Kalman filter (EnKF) is a data assimilation method that can be implemented to constrain geophysical systems (Evensen, 2003). We redirect the reader to Mathiot et al. (2012) and Massonnet et al. (2013) for a general description about how the EnKF is implemented in our ocean–sea ice model, but we repeat hereunder the two main characteristics of this filter.

The first key characteristic of the filter is to approximate the forecast error covariance matrix using a finite number of model forecasts, instead of explicitly forwarding this matrix in time. In our case, we let 25 members evolve in time, each with a perturbed version of the atmospheric forcing (Mathiot et al., 2012) as to generate ensemble spread. The second key characteristic of the EnKF lies in its multivariate formalism: any single element of the ocean–sea ice vector is updated, with a proportionality factor that is changing with time and space, this factor being precisely prescribed in the forecast error covariance matrix.

The update of the whole state vector is a non-trivial problem when data assimilation is applied to ocean–sea ice models (Lisæter et al., 2003). As an example, we display in Fig. 1 the correlations between NEMO-LIM3 sea ice concentration and mean grid cell thickness, obtained from an ensemble of 25 members each subject to a perturbation in the atmospheric forcing. In winter (left panel), the relationship is positive in the marginal ice zone. This is about where the 0°C isotherm lies in the atmospheric forcing; members that undergo cold conditions in the marginal zones will then grow more ice, resulting in an increase in both concentration and thickness. In late summer however (right panel of the figure), the correlations may become negative. When new and thin ice forms alongside thick and multi-year ice during freeze-up, the average thickness will be lower if the thin ice is more extensive (Lisæter et al., 2003). The total ice concentration may also decrease and the total thickness increase in the presence of ridging, a process that is simulated in our model. In any case, the correlations reported in Fig. 1 point towards the fact that the relationships between ice concentration and thickness are complex since the sign of the relationship depends on space and time.

In this study, no sea ice thickness data are assimilated. We assimilate only satellite-retrieved observations of sea ice concentration from the Ocean and Sea Ice Satellite Application Facility (Eastwood et al., 2011). These reprocessed products include space- and time-varying estimates of uncertainties, which are required in the EnKF scheme. The products were interpolated on the ORCA2 grid, between January 1979 and October 2009 (they will become operational on a real-time basis soon). The ocean–sea ice state is updated every 5 days. In order to prevent ensemble collapse, we perform a localized analysis (Sakov and Bertino, 2010), with a

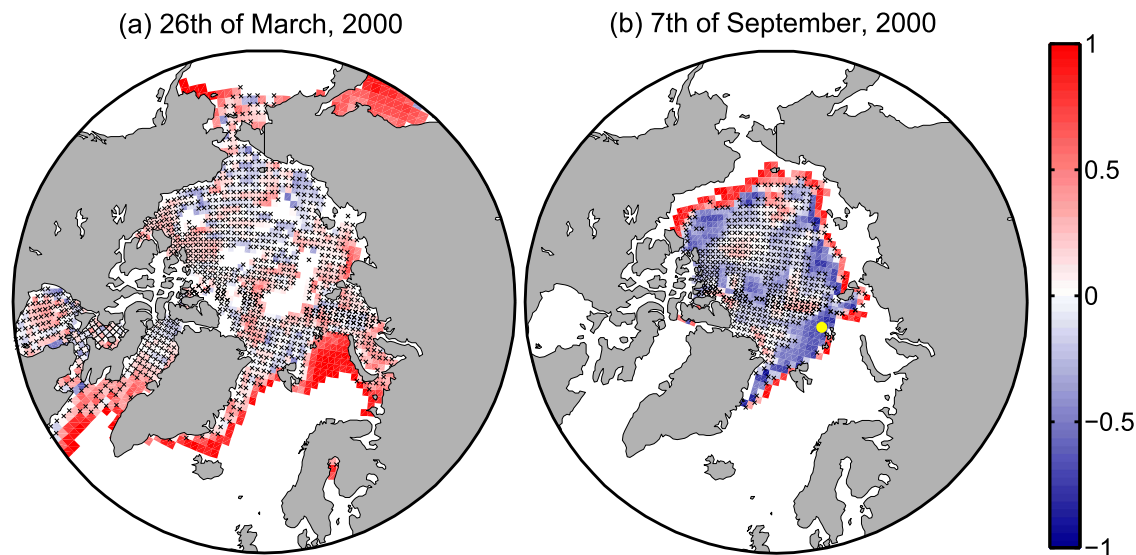


Fig. 1. Correlation between total sea ice concentration and mean thickness in the ocean–sea ice model NEMO-LIM3, for (left) the 26th of March 2000, and (right) the 7th of September 2000. Correlations are obtained from an ensemble of 25 forecasts, each forced with a different atmospheric forcing (the 10-m winds and 2-m air temperatures are perturbed, see Mathiot et al. (2012) for detailed information about the way the perturbations are created). The grid cells are stippled (\times) when correlations are not significant, that is, when associated p -values lie above the 5% level obtained using a double-sided t -test with 23 degrees of freedom. The yellow dot denotes a control grid cell used to explain, later in the text, how the EnKF analysis is conducted in the multi-category sea ice framework. Note that, in the model, the mean sea ice thickness is diagnosed from the ice-covered part of the grid cell, thus excluding open water in the calculation.

Table 1

List of sea ice and ocean variables updated after the ensemble Kalman filter analysis. The superscript c is used for sea ice variables defined for the five ice thickness categories.

Sea ice model	Ocean model
Concentration ^c	Turbulent kinetic energy
Ice volume per unit area ^c	Temperature
Snow volume per unit area ^c	Salinity
Brine content ^c	Relative vorticity
Age ^c	Horizontal divergence
Velocity (u -component)	Velocity (u -component)
Velocity (v -component)	Velocity (v -component)
Basal heat flux (solar contribution)	Sea surface height

localization radius of 800 km. This value is consistent with the recent finding by Blanchard-Wrigglesworth and Bitz (2014) that the spatial scale for decorrelation of sea ice thickness has typical values between 500 and 1000 km in the Arctic. Due to the finite number of members (25) used during data assimilation, the forecast error structure is not entirely captured and relationships between assimilated and non-assimilated variables may be represented incorrectly. We are confident that the basic relationship between ice concentration and thickness is well represented in our ensemble (Fig. 1) but acknowledge that other variables, including sea surface temperature (SST), sea surface salinity (SSS) or snow thickness, may be updated not adequately after each analysis.

This study is, to our knowledge, the first one to implement the EnKF in a sea ice model with multiple ice thickness categories. However, the observations of ice concentration used in the present study are only available at the grid cell level, and not for each ice thickness category. We perform the analysis step individually for each sea ice and snow variable in each ice thickness category (Table 1), except ice and snow heat contents (Mathiot et al., 2012) that we update separately after the EnKF analysis. That is, each variable at the sub-grid scale level is updated according to its relationship with the total ice concentration in the model (i.e., the variable that is assimilated). Fig. 2 illustrates how sea ice

thickness is updated for each ice category individually given an observation of sea ice concentration for the entire grid cell. It is expected that the filter would be more efficient if ice concentration was assimilated for each ice category individually. However, observational estimates of sea ice concentration per thickness category do not exist, to our knowledge, to constrain large-scale sea ice models.

After the statistical update of the ocean and sea ice states by the filter, physical consistency is not guaranteed. Total ice concentration may exceed 100%, sea ice thickness in each category may be out of the bounds prescribed in the model, or the sea surface temperature may be updated below its freezing point. To handle these pathological cases, we repeat the following “sanity check” after each update by the EnKF to ensure that the system is balanced before a new forecast cycle is started:

1. Reset the sea ice prognostic variables to zero if the analyzed total concentration is less than zero.
2. Update the sea ice and snow heat contents in each layer of each category proportionally to the corresponding ice and snow volume changes in the same layer and category.
3. Rebin ice categories: ice and snow areas, volumes and heat contents are transferred to neighboring categories in case ice thickness exceeds the bounds of the current ice category.
4. Shrink the ice: if total concentration exceeds 1, reduce the area of each ice category proportionally to its original areal contribution.
5. Rebin ice categories (same as 3.), as sea ice thickness may have changed in 4.
6. Reset sea surface temperature to freezing point of seawater if sea surface temperature is below the freezing point (the freezing point of seawater in OPA9 is a function of sea surface salinity).

Note that seawater salinity is updated during the EnKF analysis but not corrected during the sanity check. Still, a weak restoring towards the Levitus, 1998 sea surface salinities is applied as discussed in Mathiot et al. (2012).

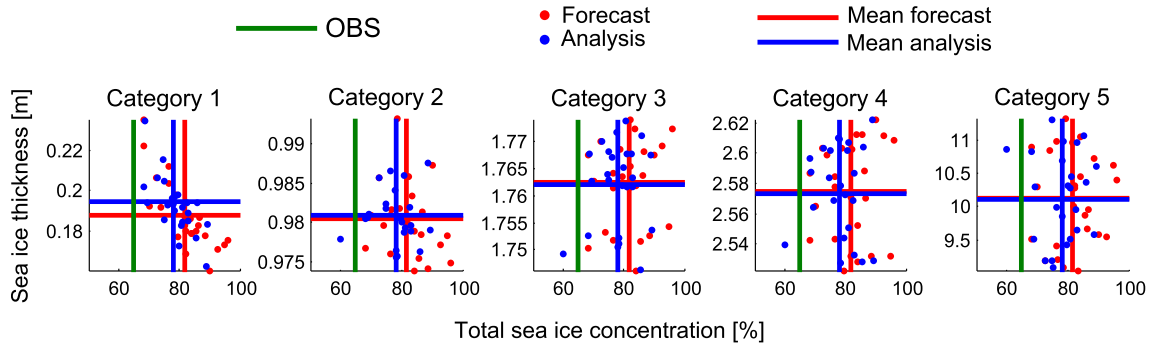


Fig. 2. Update of sea ice thickness by the ensemble Kalman filter in the multi-category sea ice model LIM3. Consider the grid cell marked with a yellow dot in Fig. 1(b). The total (sum over the five categories) sea ice concentration in this grid cell from the 25 ensemble forecasts is plotted, for each category, against sea ice thickness in the category (red dots). The means of the forecasts are shown by red lines. The observed total sea ice concentration is denoted by the vertical green line. For each category, sea ice thickness is updated (blue dots) for each member depending on the relationship between thickness and total concentration in the ensemble. In this example, sea ice thickness undergoes the largest updates in category 1. Indeed, a strong negative relationship ($r = -0.81$) prevails in this category between sea ice thickness and total concentration. Since the model total concentration overestimates the observed one, sea ice becomes thicker in this category. The update is conducted similarly for all other variables of the sea ice model, including ice concentration in each category. (For interpretation of the references to color in this figure legend, the reader is referred to the web version of this article.)

2.3. Setup

In order to test the sensitivity of seasonal prediction skill to initial conditions, two sets of ocean–sea ice initial conditions were created. The first set was obtained by running our ocean–sea ice model between 1979 and 2009 without data assimilation (Section 2.1). This run is labeled ‘CONTROL’ in Fig. 3 and is represented by the thick, continuous red line. The other set of initial conditions were obtained from the data assimilation experiment described in Section 2.2. The average of the 25 analyzed members was considered as the best estimate of the ocean–sea ice state. This is denoted by ‘ASSIM’ in Fig. 3 and represented by the thick, continuous blue line.

A pair of retrospective seasonal predictions were then considered for each year between 1983 and 2009.¹ These predictions are represented by the thin, blue and red lines starting from thick dots in Fig. 3. The ‘CONTROL’ seasonal hindcast of a given year starts the 25th of February of that year (aka “March initialization”) from the ‘CONTROL’ ocean and sea ice restarts. The ‘INITIALIZED’ seasonal hindcast also starts the 25th of February of that year but from the ‘ASSIM’ ocean and sea ice restarts. While the ‘CONTROL’ seasonal hindcasts are indistinguishable from the ‘CONTROL’ run since the atmospheric forcing and initial conditions are identical, the ‘INITIALIZED’ seasonal hindcasts will depart from the ‘ASSIM’ experiment since data assimilation is no longer activated during these hindcasts.

We remind the reader that both control and initialized ocean–sea ice simulations are, at all times, driven by atmospheric reanalyses and climatologies. We deliberately designed this setup to test, under identical and controlled atmospheric conditions, the sensitivity of September sea ice prediction skill to initial winter conditions. Our task is now to evaluate the skill of these pairs of predictions for each year between 1983 and 2009.

Our primary metric for evaluation of seasonal hindcasts quality is the Root Mean Squared Error (RMSE) of sea ice concentration a , at time t :

$$\text{RMSE}(t) = \sqrt{\frac{1}{N} \sum_{i=1}^N w_i (a(t)_i^{\text{OBS}} - a(t)_i^{\text{MOD}})^2}$$

¹ We decided to exclude the years 1979–1982 from our analysis (1) to let NEMO-LIM3 adjust to the constraint imposed by the EnKF and (2) because of a known warm bias in the NCEP/NCAR reanalysis in the early 1980s in the Beaufort and Laptev Seas.

where $i = 1, \dots, N$ runs for the grid point index, and the w_i ’s are the weights ensuring consistent weighting by the grid cell area. Only the grid points that were sensed by the satellite are considered in the calculation. Thus, the number of grid points N varies from day to day, depending on the satellite coverage. We express ice concentrations in % of the grid cell area and the RMSE is therefore expressed in %, too. The superscripts MOD and OBS refer to total ice concentration as diagnosed daily by the sea ice model (LIM3) and retrieved from satellite observations (Eastwood et al., 2011), respectively. The RMSE is by definition positive, and will increase wherever the modeled and observed sea ice concentrations differ from each other. The RMSE as a metric is insightful because it does not allow model forecast errors to compensate spatially, as is the case if sea ice area or extent are used (Notz, 2013).

3. Results

We show in Fig. 4 the evolution of the average 1983–2009 RMSE in sea ice concentration for the initialized and uninitialized seasonal hindcasts. In the first month of the hindcasts, the initialized simulation is by definition subject to a lower forecast error than the control simulation. The skill is lost within the three first months of the hindcasts, but the memory from initial conditions reemerges in August and September. These differences in RMSE scores in summer are entirely due to differences in initial conditions, since the atmospheric forcing is identical in each pair of seasonal hindcasts. The RMSE of the initialized simulation then returns to the control RMSE for the next winter. We diagnosed notable reductions of RMSE even 18 months after initialization (not shown here): in 73% of the cases, the RMSE of the initialized run was lower than the control RMSE in September of next year after the initialization.

The RMSE scores provided in Fig. 4, averaged over 1983–2009, may filter out year-to-year variations. Therefore, we plot in Fig. 5, the model forecast error in September ice concentration obtained from the control and initialized runs, for each year between 1983 and 2009. In line with the results of Fig. 4, the skill of September sea ice concentration is generally higher (the RMSE is lower) in the initialized hindcasts than in the control hindcasts. The average reduction in RMSE is small and not significant at two standard deviations for hindcasts spanning the period 1983–1999 ($0.8 \pm 1.4\%$) but is larger and significant over 2000–2009 ($3.1 \pm 2.5\%$). In some years of the last decade of the simulations, the departure from the control run is particularly marked, with

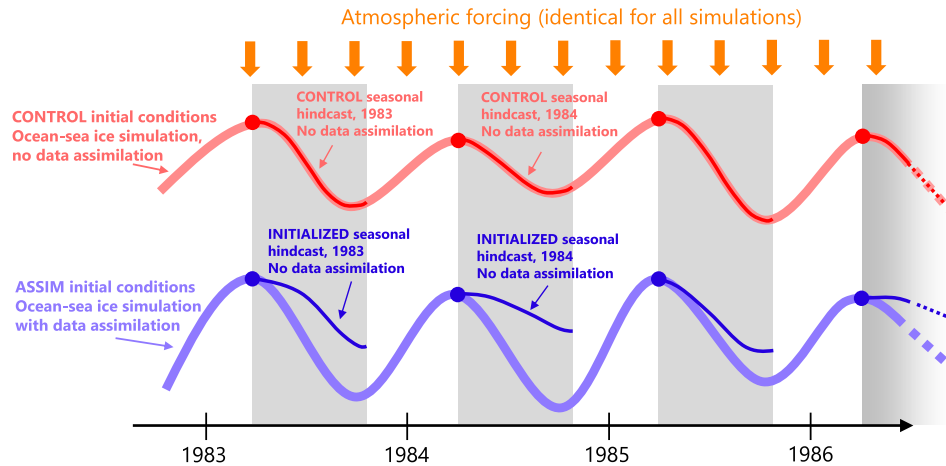


Fig. 3. Schematic description of the experimental setup of this study. (1) Two 1979–2009 ocean–sea ice simulations forced by atmospheric reanalyses and climatologies are conducted (see the text for details about the atmospheric forcing). The first one is represented by the continuous thick, light-red line at the top: it consists in a run without data assimilation. The second one (represented by the continuous, thick light-blue line at the bottom) consists in a run with data assimilation of sea ice concentration. (2) For each year between 1983 and 2009, we branch two seasonal hindcasts with initial conditions taken from the two runs described in (1), driven by the same atmospheric forcing as in (1) but with data assimilation turned off in both cases. These seasonal hindcasts are represented by the red and blue thin lines starting from a dot (•), respectively. (For interpretation of the references to color in this figure legend, the reader is referred to the web version of this article.)

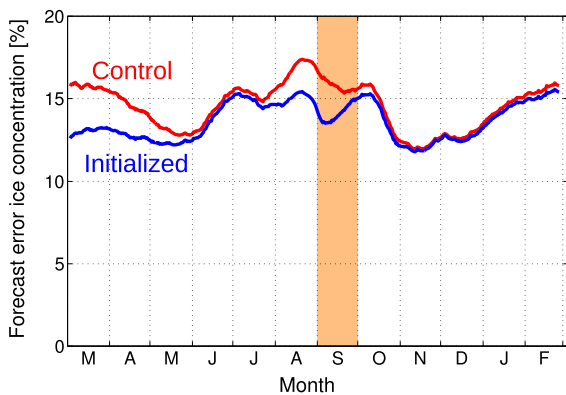


Fig. 4. Evolution of average (1983–2009) model forecast error in Arctic sea ice concentration starting in March (time of the initialization) during the first year of the simulations. The model forecast error is defined as the RMSE between simulated and observed (Eastwood et al., 2011) concentrations. Lower values indicate higher skill. The lower line (blue) corresponds to the RMSE of the run initialized every month of March, while the upper (red) line is the RMSE of the control run. The vertical orange bands highlight the month of September, that is the target month for prediction. (For interpretation of the references to color in this figure legend, the reader is referred to the web version of this article.)

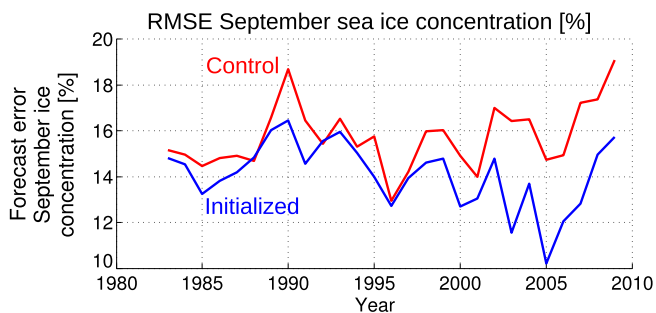


Fig. 5. (a) Average model forecast error (RMSE) of sea ice concentration in September, from initialized runs (blue) and the control run (red). As for Fig. 4, the RMSE is calculated against the observed concentrations of Eastwood et al., 2011. Pay attention that the lower value of the y axis is set to 10% to ensure readability. (For interpretation of the references to color in this figure legend, the reader is referred to the web version of this article.)

the RMSE dropping from 15% to 10% in 2005 and from 17% to 13% in 2007, for example. In Section 4, we will discuss the possible reasons why the reductions in RMSE could be larger in the last decade than in the two first decades.

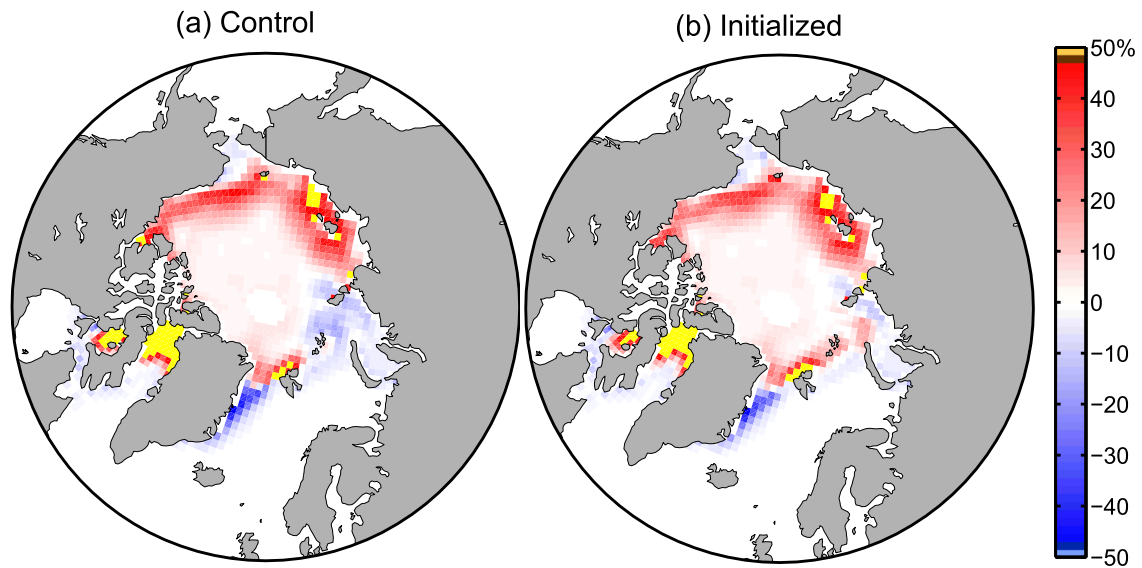
Fig. 6 shows the spatial distribution of the bias in September sea ice concentration over 1983–1999 and 2000–2009, in the seasonal hindcasts. Consistently with the RMSE time series for September (Fig. 5), hardly no difference can be detected up to the late 1990s. The largest differences occur between 2000 and 2009. The bias in the control simulation exhibits a dipole: overestimation in the Beaufort and Chukchi Seas and underestimation in the Barents and Kara Seas. The origin of such a dipole is not clear yet, but has been identified for sea ice thickness in another sea ice model (Hunke, 2014) driven by a modified NCEP forcing. The negative bias in sea ice concentration is partly suppressed in the initialized runs for the Barents and Kara Seas, suggesting a role of initial conditions there. The bias is not significantly reduced in the Beaufort and Chukchi Seas.

For the sake of completeness, we also present in Fig. 7 the inter-annual evolution of September Arctic sea ice extent as simulated by the control and initialized runs. Sea ice extent is calculated as the sum of grid cell areas where ice concentration is larger than 15%. Therefore, it does not allow to measure whether or not the simulated ice cover has correct spatial patterns. In fact, minor changes are noticed between the control and initialized runs: for example, the detrended correlation of September sea ice extent with the observations is 0.83 in the control run, and 0.89 in the initialized run. It is also interesting to note that the extent in September 2007 is the same in observations and in the two simulations, but that a pointwise comparison does indicate a difference between those two simulations (Fig. 5). We discuss in more details the simulation of the 2007 Arctic sea ice minimum in the next section.

4. Discussion

The evolution of model forecast error in the few months after initialization (Fig. 4) highlights that sea ice initialization is beneficial during the first three months following the initialization date, but also in summer. In other words, the information from surface conditions persists for about three months (March–May),

September 1983-1999 model - observed ice concentration



September 2000-2009 model - observed ice concentration

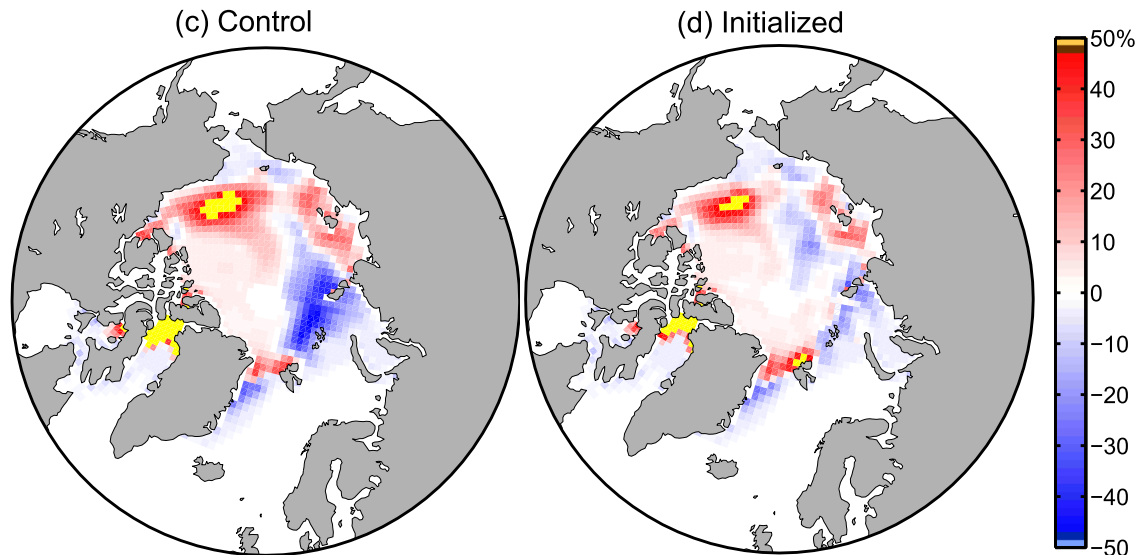


Fig. 6. Average modeled minus observed (Eastwood et al., 2011) sea ice concentration over the months of September for two time periods: 1983–1999 (a,b) and 2000–2009 (c,d). The left panels (a,c) correspond to the control seasonal hindcasts (no initialization from data assimilation) while the right panels (b,d) correspond to the seasonal hindcasts initialized from data assimilation. Notice the absence of data around the North Pole, where retrievals from satellites have not been possible.

disappears temporarily (June–July) but reemerges at the end of the melt season (August–September). Bearing in mind that our simulations do not include an interactive atmospheric model but are rather conducted under prescribed atmospheric conditions, we suggest the following explanations to interpret Fig. 4:

- From March to May right after the initialization, the RMSE of the initialized simulations gets closer to the reference RMSE. The sea ice concentrations are nearly identical in both simulations because they approach 100% wherever the prescribed 2-m air temperatures are below the seawater freezing point. That is, in our setup, sea ice concentration is highly constrained by the imposed atmospheric forcing when surface temperatures are negative.
- In June and July, surface air temperatures start to rise above the sea ice melting point. Sea ice concentration decreases first in the marginal zones, where ice is thin. The small differences in sea ice thickness provided by the EnKF initialization in the marginal ice zone may delay/advance the timing of ice retreat by a few days, but not significantly to have clear impacts on the RMSE in spring.
- In August and September, the whole Arctic basin is experiencing positive surface air temperatures. In a study using NEMO-LIM3, Goosse et al. (2009) related the probability that an ice parcel melts completely in late summer to its average thickness in April. Below 1.24 m (above 2.33 m), they found this probability to be larger than 90% (lower than 10%) based on a 1979–2006 simulation. We suggest that the updates in sea ice thickness

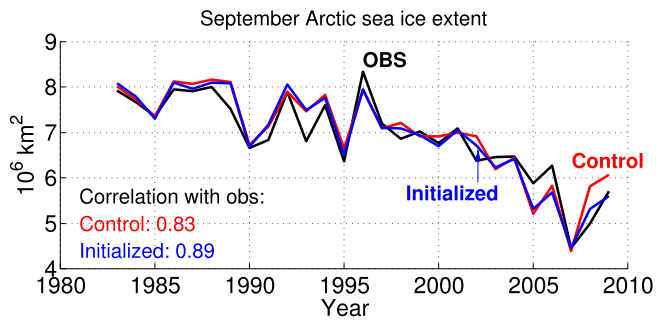


Fig. 7. September Arctic sea ice extent, calculated as the sum of all grid cell areas where sea ice concentration exceeds 15%. Observational data are from [Comiso and Nishio \(2008\)](#). The red line is the sea ice extent from the control simulation, the blue line shows the ensemble of September sea ice extent hindcasts obtained when initialized in March the same year, and the black line is the observed September sea ice extent ([Comiso and Nishio, 2008](#)). The correlations reported in the lower-left corner of the figure have been calculated after detrending all time series. (For interpretation of the references to color in this figure legend, the reader is referred to the web version of this article.)

provided by the EnKF can shift local ice thickness in either the thin (<1.24 m) or thick (>2.33 m) categories, thereby changing the fate of sea ice concentration in late summer.

- From October to February of the next year, sea ice concentration rapidly grows to 100% wherever the surface air temperatures are below the seawater freezing point, regardless of the sea ice thickness.

As reported in [Fig. 5](#), the skill of September sea ice concentration in the initialized runs departs significantly from the skill of the control runs from the late 1990s onwards. We suspect, following the arguments of [Goosse et al. \(2009\)](#), that this is intimately related to the fact that the probability for an ice parcel to melt in summer decreases nonlinearly with the average sea ice thickness. In a regime of thick (>2.33 m) ice, this probability is very low, and the updates from the assimilation do not alter significantly this probability as the ice thickness remains anyway above this limit. This is what happens up to the mid-1990s. In a regime of intermediate thickness (less than 2.33 m but larger than 1.24 m), the probability to melt decreases sharply, so that the updates from the assimilation have clear impact on the presence of ice at the end of the melt season (from the mid 1990s to 2009). Ultimately, as sea ice might become very thin (<1.24 m) in a near future, we expect again that the impact of assimilation will be small because the ice will have anyway a very high probability to melt away in September: the Arctic will be at this stage in a regime of seasonal ice.

To illustrate the role played by the winter sea ice thickness distribution on the September sea ice concentration, we pick the emblematic year of 2007. We choose this year because it is the time of the absolute minimum in sea ice extent over our period (1983–2009), but also because the spatial distribution of observed ice concentration in September 2007 was somewhat peculiar ([Fig. 8\(c\)](#), pink contour), with a long “tongue” of ice extending from Greenland to Siberia. The control run, while simulating a correct sea ice extent ([Fig. 7](#)), overestimates sea ice concentration in the Beaufort Sea and the Baffin Bay, and underestimates it between the North Pole and the Laptev Sea ([Fig. 8\(c\)](#)). The initialized run simulates a correct sea ice extent as well, but in addition shows a more realistic spatial distribution of ice ([Fig. 89f](#)). The ultimate cause for the differences between the initialized and control simulations in September must lie in the ocean and/or sea ice initial conditions, since the model was forced with the same atmospheric data in both cases. The corresponding maps of winter sea ice

thickness ([Fig. 8\(a\)](#) and (d)) reveal substantial differences up to a meter locally. It is for example straightforward to note that ice is thicker in the initialized run at the location of the “tongue” six months later, and is logically able to survive after six months. We also examined the June 2007 model output (not shown here). While sea ice concentrations were hardly distinguishable from each other, differences in sea ice thickness similar to those identified in March were noticed.

Demonstrating formally that sea ice thickness is the only variable that sustains memory in the system would require several other data assimilation experiments, and is out of the scope of the present paper. Because the ocean could be an alternative source of memory in the system, it is still interesting to look at the near-surface ocean temperature at the beginning of the two seasonal hindcasts, in March 2007 ([Fig. 8\(b\)](#) and (e)). Below the ice-covered part of the oceanic domain, differences up to 0.1 °C are noticed over the top 30 m of the ocean. For example, colder waters are found in the Barents and Kara Seas in the initialized run, where the EnKF produces thicker ice. This is consistent with the physics of the model: reduced heat content is required to allow maintaining thicker sea ice at the surface. However, these differences in ocean temperature unlikely explain the persistence of sea ice concentration six months later in the initialized run: back-of-the-envelope calculations show that the heat content associated to a difference of 0.1 °C in mean ocean temperature over a depth of 30 m, corresponds to the energy required to melt ~4 cm of ice, all other things being equal. Larger temperature differences are noted outside of the ice edge ([Fig. 8\(h\)](#)), up to 1° warmer in the initialized run east of Greenland. Examination of the maps of other years (not shown here) reveals a systematic overestimation of sea ice concentration in the control run near the ice edge. The filter corrects this bias for ice concentration and, again, updates temperatures accordingly: it increases the temperatures where ice is removed. Again, it is unlikely that the temperature differences between the initialized and uninitialized runs explain the differences in September 2007 sea ice concentration since (1) colder waters, and not warmer ones, would be expected to sustain ice in the initialized run in the Barents and Kara Seas, and (2) the warmer waters east of Greenland in the initialized run propagate southwards in the model, and not northwards (not shown here). To sum up, we have good evidence that the differences in oceanic temperature in March between the two runs are the sign that the EnKF is working correctly, but unlikely explain the differences in sea ice concentration in September.

Our setup is far from optimal and complete. By running the ocean–sea ice simulations with prescribed atmospheric fields, some important sea ice– and ocean–atmosphere feedbacks are not taken into account. In addition, the NCEP/NCAR reanalyses were themselves obtained by the assimilation of SST and sea ice concentration. It should be further assessed how the choice of the atmospheric reanalyses impacts the reconstruction of initial states used for the prediction. Regarding the data assimilation method, our ensemble is likely under-dispersive and model updates too small. Additional initialization of the ocean surface/3D temperatures/salinities would probably permit to also increase the forecast skill in winter. Actually, we ran the 27 seasonal predictions with sea ice initialization in September, but did not notice any improvement in skill for March next year (not shown here). This was to be expected, because previous studies have shown that the area and volume of sea ice in September are poor predictors for subsequent March sea ice area ([Blanchard-Wrigglesworth et al., 2011](#); [Chevallier and Salas Méliá, 2012](#)). In winter, the position of the marginal ice zone is rather controlled by ocean heat flux convergence ([Bitz et al., 2005](#)) or by atmospheric heat flow. In the same line, we did not find re-emergence of skill in the Southern Ocean sea ice (not shown here). Again, the additional initialization

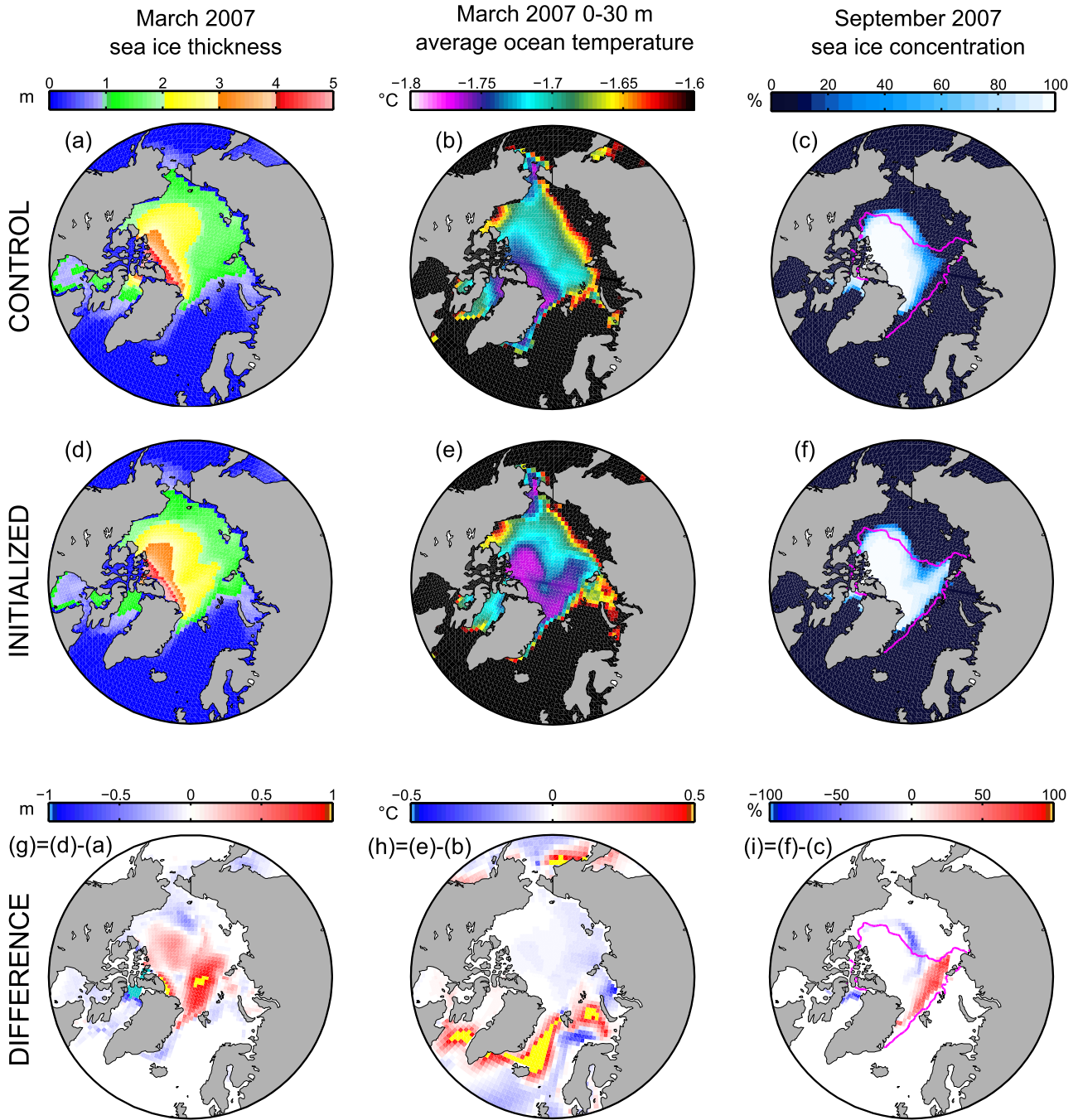


Fig. 8. (Left column) Mean sea ice thickness in March 2007 from the control run (a), the initialized run (d), and the difference (g) = (d) – (a). (Middle column) Same, for March 2007 ocean temperature averaged vertically over the top three model vertical levels. (Right column) Same, for sea ice concentration in September 2007. The pink lines in panels (c), (f) and (i) denote the 15% ice edge contour from observations (Comiso and Nishio, 2008). (For interpretation of the references to color in this figure legend, the reader is referred to the web version of this article.)

of ocean variables could, in principle, yield sea ice predictability and hopefully prediction skill in the Southern Ocean (Holland et al., 2013).

5. Conclusion

In the next decades, summer Arctic sea ice extent is expected to continue on its decline (Stroeve et al., 2012; Massonnet et al., 2012; Wang and Overland, 2012). Under reduced ice conditions, the use of historical predictor–predictand relationships, sometimes invoked for seasonal sea ice prediction (e.g., Tivy et al., 2007) may

be of limited use (Holland and Stroeve, 2011). Resorting to fully-coupled models is an appealing solution, provided that (1) these include the essential atmosphere–sea ice and ocean–sea ice feedbacks (Wang et al., 2012), and (2) they are initialized properly. Our results stress that the seasonal sea ice prediction skill may depend on the mean state, since improvements are clearly larger when ice is thinner in our setup. Such non-stationarity would be difficult to handle without the use of a dynamical model, that is, using a statistical model only.

In this work we have run ocean–sea ice hindcasts with prescribed atmospheric forcing but with different sea ice initial

conditions, which has permitted to isolate the added value of sea ice initialization for summer Arctic sea ice prediction. This study builds upon the known fact that, in a multivariate data assimilation scheme, the model sea ice thickness can be updated even if thickness is not directly assimilated into the model (Lisæter et al., 2003; Mathiot et al., 2012; Massonnet et al., 2013). Supporting this earlier finding in the context of seasonal prediction, our results have two main implications. (1) A realistic initialization of the sea ice cover is possible by simple assimilation of sea ice concentration, provided that the assimilation is conducted in a consistent multivariate framework. Initializing sea ice concentration only (as in, e.g., Sigmond et al., 2013) may be insufficient to sustain and transport memory from winter to summer (Tietsche et al., 2012). (2) For identical atmospheric conditions, predictions starting from initialized states provide more realistic sea ice areal distributions in summer, with notable improvements during the 2000s.

There are many sources of uncertainty that will hamper the realization of skillful seasonal Arctic sea ice predictions in the next years. Our results show at least that a consistent initialization of the winter sea ice conditions is necessary to provide realistic distributions of subsequent summer sea ice cover.

Acknowledgments

We thank three anonymous reviewers and the Editor for helpful comments that contributed to improve the manuscript. We thank Matthieu Chevallier for stimulating discussions. François Massonnet is a F.R.S.-FNRS Post-Doctoral Researcher. Hugues Goosse is a F.R.S.-FNRS Senior Research Associate. Computational resources have been provided by the supercomputing facilities of the Université catholique de Louvain (CISM/UCL) and the Consortium des Équipements de Calcul Intensif en Fédération Wallonie Bruxelles (CÉCI) funded by the Fond de la Recherche Scientifique de Belgique (F.R.S.-FNRS) under convention 2.5020.11. This work was partly funded by the European Commissions 7th Framework Programme, under Grant Agreement number 226520, COMBINE project (Comprehensive Modelling of the Earth System for Better Climate Prediction and Projection). It was also partly supported by the Belgian Science Federal Policy Office (BELSPO).

References

- AMAP, 2011. Snow, Water, Ice and Permafrost in the Arctic (SWIPA): Climate Change and the Cryosphere. Tech. rep., Arctic Monitoring and Assessment Programme (AMAP), Gaustadalléen 21, N-0349 Oslo, Norway (<www.amap.no>).
- Baumgartner, A., Reichel, E., 1976. The world water balance mean annual global, continental and maritime precipitation, evaporation and run-off. *Agric. Water Manage.* 1 (1), 100–101.
- Berliand, M.E., Strokina, T.G., 1980. Global distribution of the total amount of clouds. *Hydrometeorological* 71 (in Russian).
- Bitz, C., Holland, M., Hunke, E.C., Moritz, R.E., 2005. Maintenance of the sea-ice edge. *J. Clim.* 18, 2903–2921.
- Blanchard-Wrigglesworth, E., Bitz, C.M., 2014. Characteristics of Arctic sea-ice thickness variability in GCMs. *J. Clim.* <http://dx.doi.org/10.1175/JCLI-D-14-00345.1>.
- Blanchard-Wrigglesworth, E., Armour, K.C., Bitz, C.M., DeWeaver, E., 2011. Persistence and inherent predictability of Arctic sea ice in a GCM ensemble and observations. *J. Clim.* 24, 231–250.
- Chevallier, M., Salas Mélia, D., 2012. The role of sea ice thickness distribution in the Arctic sea ice potential predictability: a diagnostic approach with a coupled GCM. *J. Clim.* 25, 3025–3038.
- Chevallier, M., Salas Mélia, D., Voltaire, A., Déqué, M., Garric, G., 2013. Seasonal forecasts of the pan-Arctic sea ice extent using a GCM-based seasonal prediction system. *J. Clim.* 26 (16), 6092–6104. <http://dx.doi.org/10.1175/JCLI-D-12-00612.1>.
- Comiso, J.C., Nishio, F., 2008. Trends in the sea ice cover using enhanced and compatible AMSR-E, SSM/I and SMMR data. *J. Geophys. Res.*, 113.
- Eastwood, S., Larsen, K.R., Lavergne, T., Nielsen, E., Tonboe, R., 2011. Global sea ice concentration reprocessing – product user manual. Tech. rep., OSISAF.
- Evensen, G., 2003. The ensemble Kalman filter: theoretical formulation and practical implementation. *Ocean Dyn.* 53, 343–367.
- Goosse, H., 1997. Modelling the Large-Scale Behaviour of the Coupled Ocean–Sea-Ice System (Ph.D. thesis). Université Catholique de Louvain.
- Goosse, H., Arzel, O., Bitz, C.M., de Montety, A., Vancoppenolle, M., 2009. Increased variability of the Arctic summer ice extent in a warmer climate. *Geophys. Res. Lett.* 36, L23702.
- GRDC, 2000. Observed historical discharge data from major rivers for climate model validation. Tech. rep., Max Planck Institute. <<https://www.mpimet.mpg.de/fileadmin/publikationen/Reports/maxscirep307.pdf>>.
- Holland, M.M., Stroeve, J., 2011. Changing seasonal sea ice predictor relationships in a changing Arctic climate. *Geophys. Res. Lett.* 38, L18501.
- Holland, M.M., Blanchard-Wrigglesworth, E., Kay, J., Vavrus, S., 2013. Initial-value predictability of Antarctic sea ice in the community climate system model 3. *Geophys. Res. Lett.* 40 (10), 2121–2124. <http://dx.doi.org/10.1002/grl.50410>.
- Hunke, E.C., 2014. Sea ice volume and age: Sensitivity to physical parameterizations and thickness resolution in the ice sea ice model. *Ocean Modell.* 82 (0), 45–59 <<http://www.sciencedirect.com/science/article/pii/S1463500314000973>>.
- Kalnay, E., Kanamitsu, M., Kistler, R., Collins, W., Deaven, D., Gandin, L., Iredell, M., Saha, S., White, G., Woollen, J., Zhu, Y., Chelliah, M., Ebisuzaki, W., Higgins, W., Janowiak, J., Mo, K.C., Ropelewski, C., Wang, J., Leetmaa, A., Reynolds, R., Jenne, R., Joseph, D., 1996. The NCEP/NCAR 40-year reanalysis project. *Bull. Am. Meteorol. Soc.* 77, 437–471.
- Kauker, F., Kaminski, T., Karcher, M., Giering, R., Gerdes, R., Vobeck, M., 2009. Adjoint analysis of the 2007 all time Arctic sea-ice minimum. *Geophys. Res. Lett.* 36, L03707.
- Kwok, R., Hunke, E.C., Maslowski, W., Menemenlis, D., Zhang, J., 2008. Variability of sea ice simulations assessed with RGPS kinematics. *J. Geophys. Res.*, 113.
- Large, W.G., Yeager, S.G., 2004. Diurnal to decadal global forcing for ocean and sea-ice models: the data sets and flux climatologies. Tech. rep., NCAR.
- Laxon, S.W., Giles, K.A., Ridout, A.L., Wingham, D.J., Willatt, R., Cullen, R., Kwok, R., Schweiger, A., Zhang, J., Haas, C., Hendricks, S., Krishfield, R., Kurtz, N., Farrell, S., Davidson, M., 2013. Cryosat-2 estimates of Arctic sea ice thickness and volume. *Geophys. Res. Lett.* 40 (4), 732–737. <http://dx.doi.org/10.1002/grl.50193>.
- Levitus, S., 1998. NODC World Ocean Atlas. <<http://www.esrl.noaa.gov/psd/>>.
- Lindsay, R., 2013. Unified sea ice thickness climate data record collection spanning 1947–2012. <http://dx.doi.org/10.7265/N5D50JXV>.
- Lindsay, R., Haas, C., Hendricks, S., Hunkeler, P., Kurtz, N., Paden, J., Panzer, B., Sonntag, J., Yungel, J., Zhang, J., 2012. Seasonal forecasts of Arctic sea ice initialized with observations of the ice thickness. *Geophys. Res. Lett.* 39 (21), L21502. <http://dx.doi.org/10.1029/2012GL053576>.
- Lisæter, K.A., Rosanova, J., Evensen, G., 2003. Assimilation of ice concentration in a coupled ice–ocean model, using the ensemble Kalman filter. *Ocean Dyn.* 53, 368–388.
- Lisæter, K.A., Evensen, G., Laxon, S., 2007. Assimilating synthetic CryoSat sea ice thickness in a coupled ice–ocean. *J. Geophys. Res.* 112, C07023.
- Madec, G., 2008. NEMO ocean engine: Note du Pôle de modélisation de l'Institut Pierre-Simon Laplace No 27. <<http://www.nemo-ocean.eu/About-NEMO/Reference-manuals>>.
- Maslanik, J.A., Fowler, C., Stroeve, J., Drobot, S., Zwally, J., Yi, D., Emery, W., 2007. A younger, thinner Arctic ice cover: increased potential for rapid, extensive sea-ice loss. *Geophys. Res. Lett.* 34, L24501.
- Massonnet, F., Fichefet, T., Goosse, H., Bitz, C.M., Philippon-Berthier, G., Holland, M.M., Barriat, P.-Y., 2012. Constraining projections of summer Arctic sea ice. *Cryosphere* 6 (6), 1383–1394 <<http://www.the-cryosphere.net/6/1383/2012/>>.
- Massonnet, F., Mathiot, P., Fichefet, T., Goosse, H., König Beatty, C., Vancoppenolle, M., Lavergne, T., 2013. A model reconstruction of the Antarctic sea ice thickness and volume changes over 1980–2008 using data assimilation. *Ocean Modell.* 64, 67–75 <<http://www.sciencedirect.com/science/article/pii/S146350031300005X>>.
- Mathiot, P., König Beatty, C., Fichefet, T., Goosse, H., Massonnet, F., Vancoppenolle, M., 2012. Better constraints on the sea-ice state using global sea-ice data assimilation. *Geosci. Model Dev.* 5 (6), 1501–1515 <<http://www.geosci-model-dev.net/5/1501/2012/>>.
- Notz, D., 2013. Sea-ice extent provides a limited metric of model performance. *Cryosphere Discuss.* 7, 3095–3131.
- Sakov, P., Bertino, L., 2010. Relation between two common localisation methods for the EnKF. *Comput. Geosci.* 15 (2), 225–237.
- Schweiger, A., Lindsay, R., Zhang, J., Steele, M., Stern, H., Kwok, R., 2011. Uncertainty in modeled Arctic sea ice volume. *J. Geophys. Res.* 116, C00D06.
- Sigmond, M., Fyfe, J.C., Flato, G.M., Khari, V.V., Merryfield, W.J., 2013. Seasonal forecast skill of Arctic sea ice area in a dynamical forecast system. *Geophys. Res. Lett.* 40 (3), 529–534. <http://dx.doi.org/10.1002/grl.50129>.
- Stroeve, J.C., Kattsov, V., Barrett, A., Serreze, M., Pavlova, T., Holland, M., Meier, W.N., 2012. Trends in Arctic sea ice extent from CIMP5, CIMP3 and observations. *Geophys. Res. Lett.* 39 (16), L16502. <http://dx.doi.org/10.1029/2012GL052676>.
- Stroeve, J., Hamilton, L.C., Bitz, C.M., Blanchard-Wrigglesworth, E., 2014. Predicting september sea ice: ensemble skill of the search sea ice outlook 2008–2013. *Geophys. Res. Lett.* <http://dx.doi.org/10.1002/2014GL059388>.
- Tietsche, S., Notz, D., Jungclaus, J.H., Marotzke, J., 2012. Assimilation of sea-ice concentration in a global climate model – physical and statistical aspects. *Ocean Sci. Discuss.* 9 (4), 2403–2455 <<http://www.ocean-sci-discuss.net/9/2403/2012/>>.
- Tivy, A., Alt, B., Howell, S., Wilson, K., Yackel, J., 2007. Long-range prediction of the shipping season in hudson bay: a statistical approach. *Weather Forecast.* 22 (5), 1063–1075. <http://dx.doi.org/10.1175/WAF1038.1>.
- Trenberth, K.E., Large, W., European Centre for Medium Range Weather Forecasts, 1989. A global ocean wind stress climatology based on the ECMWF analyses. <<http://dss.ucar.edu/datasets/ds110.1/>>.

- Vancoppenolle, M., Fichefet, T., Goosse, H., Bouillon, S., Madec, G., Morales Maqueda, M.A., 2009. Simulating the mass balance and salinity of Arctic and Antarctic sea ice. 1. Model description and validation. *Ocean Modell.* 27, 33–53.
- Wang, M., Overland, J.E., 2012. A sea ice free summer Arctic within 30 years: an update from cmip5 models. *Geophys. Res. Lett.* 39 (18), L18501. <http://dx.doi.org/10.1029/2012GL052868>.
- Wang, W., Chen, M., Kumar, A., 2012. Seasonal prediction of Arctic sea ice extent from a coupled dynamical forecast system. *Mon. Weather Rev.* 141 (4), 1375–1394. <http://dx.doi.org/10.1175/MWR-D-12-00057.1>.
- Zhang, J., Steele, M., Lindsay, R., Schweiger, A., Morison, J., 2008. Ensemble 1-year predictions of Arctic sea ice for the spring and summer of 2008. *Geophys. Res. Lett.*, 35.
- Zygmuntowska, M., Rampal, P., Ivanova, N., Smedsrud, L.H., 2014. Uncertainties in Arctic sea ice thickness and volume: new estimates and implications for trends. *Cryosphere* 8 (2), 705–720 <http://www.the-cryosphere.net/8/705/2014/>.